Plasticity, crack initiation and defect resistance in alkali-borosilicate glasses: From normal to anomalous behavior

R. Limbach [a], A. Winterstein-Beckmann [a], J. Dellith [b], D. Möncke [a], L. Wondraczek [a,*]

[a] Otto Schott Institute of Materials Research, University of Jena, Fraunhoferstrasse 6, 07743 Jena, Germany
[b] Leibniz Institute of Photonic Technology IPHT, Albert-Einstein-Straße 9, 07745 Jena, Germany

ABSTRACT

We provide a comprehensive description of the defect tolerance of sodium-borosilicate glasses upon sharp contact loading. This is motivated by the key role which is taken by this particular glass system in a wide variety of applications, ranging from electronic substrates, display covers and substrates for biomedical imaging and sensing to, e.g., radioactive waste vitrification. The present report covers the mechanical properties of glasses in the $Na_2O–B_2O_3–SiO_2$ ternary over the broad range of compositions from pure SiO_2 to binary sodium-borates, and crossing the regions of various commercially relevant specialty borosilicate glasses, such as the multi-component Duran-, Pyrex- and BK7-type compositions and typical soda-lime silicate glasses, which are also included in this study. In terms of structure, the considered glasses may be separated into two groups, that is, one series which contains only bridging oxygen atoms, and another series which is designed with an increasing number of non-bridging oxygen ions. Elastic moduli, Poisson ratio, hardness as well as creep and crack resistance were evaluated, as well as the contribution of densification to the overall amount of indentation deformation. Correlations between the mechanical properties and structural characteristics of near- and mid-range order are discussed, from which we obtain a mechanistic view at the molecular reactions which govern the overall deformation reaction and, ultimately, contact cracking.

© 2015 The Authors. Published by Elsevier B.V. This is an open access article under the CC BY license (http://creativecommons.org/licenses/by/4.0/).

1. Introduction

Multi-component alkali-borosilicates represent one of the most prominent types of specialty glasses. They are an indispensable component in a wide variety of technical applications such as substrates in electronic devices or displays, household or laboratory ware, or cover glasses [1–3]. For example, they enable relatively high softening temperatures and low coefficient thermal expansion (or also matching the coefficient of thermal expansion to that of silicon), but also very specific mechanical properties [4]. This has made them a key substrate material for silicon-based electronic circuits and, e.g., photolithographic masks. Furthermore, a high transmission in the UV and low susceptibility to defect formation designate low alkali borosilicate glasses as a very suitable material for high performance optics. The comparably weak auto-luminescence has also resulted in dedicated applications as substrate for biomedical imaging and sensing. Due to their comparably high chemical and thermo-shock resistance, hardness and fracture toughness, they are also considered for waste immobilization [5,6]. At present, the understanding of the correlation between intrinsic strength, structure and mechanical properties is the key factor in the further advancement of design tools

for such glasses [4,7–9]. Depending on composition, temperature or pressure, B_2O_3 containing glasses show severe structural changes, i.e., the change from three-fold (B_3) to four-fold coordinated boron (B_4), and also distinct variations of structural homogeneity [10–18]. This prevents simplistic theoretical approaches towards correlations between mechanical properties and intrinsic material characteristics [19]. Nevertheless, some models allow, up to a certain degree, the estimation of specific mechanical properties (like Young's modulus). Such a correlation was established by Phillips and later extended by Williams and Scott for alkali-free high-modulus glasses [20,21]. Their model is based on the assumption that the elastic modulus is changed in an additive manner by chemical composition. Another approach was proposed by Soga et al. [22], who correlated the packing density with the mechanical properties based on a mathematical equation representing the potential between two charged particles. Similar to this model, Bridge et al. [23] have taken the cation–anion stretching force constants to estimate elastic properties for many different network formers. Nevertheless, all these approaches regard only first neighbor influences and are therefore restricted to within certain limits. The simplistic temperature-dependent bond constraint theory as derived by Mauro and Gupta [24] on the basis of Phillips and Thorpe's topological constraint theory [25], tries to integrate the short- and mid-range architecture as defined by the presence of structural constraints, resulting in surprisingly good theoretical predictions of

* Corresponding author.
E-mail address: lothar.wondraczek@uni-jena.de (L. Wondraczek).

experimental hardness data [26–29]. More unifying efforts have been made by Rouxel et al., who tried to correlate mechanical properties such as elastic modulus and Poisson ratio to structural parameters such as the structural dimensionality, the free volume, the atomic packing density C_g, or the volume density of energy [6,30]. However, the present understanding of the mechanical response and, specifically, deformation processes in borosilicate glasses is still dominated by approximate and phenomenological expression such as, e.g., the notion of normal and anomalous behavior for describing shear and compaction-driven deformation procedures, respectively [31].

The ternary diagram of alkali-borosilicate glasses is quite complex, and offers different areas of interest. To differentiate between certain structural species that are dominant in certain compositions, two values have been established on the basis of molar composition, $R = Na_2O/B_2O_3$ and $K = Si_2O/B_2O_3$. Based on NMR data, Bray et al. [10] postulated a first model, which enabled the estimation of the fraction of fourfold coordinated boron ($N_4 = B_4/(B_3 + B_4)$) and the number of non-bridging oxygen ions in the silica sub-network (NBO_{Si}), from the R-value, that is, from the amount of network modifier oxides. Addition of modifier oxides to borate glasses or borosilicate glasses with $R < 0.5$ initially creates charged $[B\varnothing_4]^-$ tetrahedra from neutral trigonal $B\varnothing_3$ groups in pure vitreous B_2O_3 (where Ø stands for bridging oxygen atoms). That is, in contrast to vitreous SiO_2, which becomes more depolymerized with the addition of any amount of modifier oxide, the network connectivity in borate-containing glasses initially increases. However, higher modifier oxide concentrations ($R > 0.5$) cause NBO to form on trigonal borate groups, and/or on silicate tetrahedra. This coordination change makes borate containing glass systems very interesting for studying the material's response to indentation deformation, as the network can be manipulated with respect to the degree of polymerization, not only considering the number of non-bridging oxygen ions, but also considering the BO_3/BO_4 ratio [32–34].

In the present study, we provide systematic data on the elastic properties, Poisson ratio, hardness, the relation between densification and volume conservative shear flow, and correlations to damage tolerance for a range of compositions of the well investigated alkali-borosilicate system [11,12,34]. We focus on variations of the R- and K-values, i.e., BO_3/BO_4 ratios and also varying amounts of NBO, within the technologically most relevant part of the ternary (which also contains the regions of immiscibility). These data are discussed in the context of short- and mid-range structure.

2. Experimental

2.1. Glass preparation

Glasses from the sodium-borosilicate system were prepared from high purity (optical grade) raw materials (SiO_2, $CaCO_3$, Na_2CO_3, H_3BO_3). Batches of 100–250 g were melted in Pt or Pt-Rh20 crucibles in a conventional muffle furnace, with melting temperatures between 800 and 1750 °C, depending on the silica content. The KBS glass was prepared by melting batches of 4 l in a Pt crucible for 8 h at 1630 °C. To avoid phase separation, Al_2O_3 was added as $Al(OH)_3$ to the silica-rich glasses (NBS2, Duran, LBS and KBS). To ensure homogenous melts, the glasses with SiO_2 contents higher than 70 mol% were quenched in water and re-melted after drying. All melts were poured into preheated graphite molds (~20–50 K above the glass transition temperature) and cooled down to room temperature at a rate of 30 K/h, except for the Duran-type composition, which was cooled in the crucible, and the model glasses NBS A, C and D, which were quenched down to room temperature [33,34]. For comparison, commercially available SiO_2 (Suprasil, Heraeus Quarzglas GmbH & Co. KG) was analyzed as well.

Details on the glass compositions and their melting parameters are listed together with elected physical properties in Table 1. The glass transition temperature T_g was determined by differential scanning calorimetry (DSC) and the density ρ was measured by the Archimedes method, using ethanol and distilled H_2O, respectively, as immersion liquid. All experiments were conducted in laboratory air at an ambient temperature of around 25 °C.

2.2. Ultrasonic echography

The elastic properties were investigated by ultrasonic echography using an echometer (Echometer 1077, Karl Deutsch GmbH & Co KG) equipped with a piezoelectric transducer ($f = 8$–12 MHz), for the determination of the longitudinal t_L and transversal t_T sound wave propagation time with an accuracy of ± 1 ns. Prior to the measurements the glass specimens were polished co-planar to an optical finish and the exact thickness d of the 1–2 mm thin plates was measured with an accuracy of ± 2 μm using a micrometer screw. The longitudinal $c_L = 2d/t_L$ and transversal wave velocities $c_T = 2d/t_T$ were obtained from the specimen thickness and the time between two consecutive

Table 1

Nominal compositions, preparation conditions (melting temperature T_m and annealing temperature T_{cast}), and physical properties, including the fraction of $[B\varnothing_4]^-$ units N_4, glass transition T_g, density ρ and atomic packing density C_g, of the investigated glasses. Data on T_g and ρ are taken from Refs. [33–35].

	2N8B	NBS A	NBS B	NBS C	NBS D	NBS1	NBS2	Duran	BK7	LBS	KBS[a]	NCS	SiO₂
SiO_2 (mol%)	–	25.0	48.5	42.5	60.0	74	74.0	81.5	74	81.5	72.6	74	100
B_2O_3 (mol%)	80	62.5	48.5	42.5	33.5	16	20.7	11.8	16	11.8	19.0	–	–
Na_2O (mol%)	20	12.5	3.0	15.0	6.5	10	4.3	5.4[b]	10	5.4[b]	6.4[b]	10	–
Al_2O_3 (mol%)	–	–	–	–	–	–	1.0	1.3	–	1.3	2.0	–	–
CaO (mol%)	–	–	–	–	–	–	–	–	–	–	–	16	–
K (SiO_2/B_2O_3)	–	0.40	1.00	1.00	1.79	4.63	3.57	6.91	4.63	6.91	3.82	–	–
R (Na_2O/B_2O_3)	0.25	0.20	0.06	0.35	0.19	0.63	0.21	0.46	0.63	0.46	0.24	–	–
N_4 (B)[c]	0.28	0.20	0.06	0.35	0.19	0.82	0.20	–	0.82	–	0.35	–	–
OH^- (mol%)[d]	0.400	0.190	–	0.210	0.160	0.120	0.180	0.250	–	0.120	0.140	–	0.003
T_g (°C) ± 2 K	412	415	380	490	445	550	442	540	550	489	523	530	1130
T_m (°C) ± 2 K	1200	1580	1300	1300	1580	1450	1750	1750	1450	1750	1630	1450	2000
T_{cast} (°C) ± 2 K	500	–	500	–	–	600	500	600	600	600	–	600	–
ρ (g/cm³) $\pm 0.2\%$	2.07	2.18	2.04	2.31	2.15	2.45	2.18	2.22	2.45	2.14	2.26	2.48	2.20
C_g	0.521	0.532	0.485	0.534	0.490	0.528	0.479	0.462	0.485	0.490	0.480	0.528	0.457

[a] Glass composition was determined experimentally by Energy Dispersive X-Ray Spectroscopy (EDX).

[b] The values include 0.5 mol% K_2O in Duran, 5.4 mol% Li_2O in LBS and 0.8 mol% Li_2O as well as 4.9 mol% K_2O in KBS.

[c] NMR results for 2N8B, NBS1, NBS2, KBS and BK7 were taken from Refs. [11,36,37]. Values for NBS A, NBS B, NBS C and NBS D are from http://www.icglass.org/technical_committees/?id=1&committee=TC03:_Glass_Structure.

[d] The OH⁻ content was calculated from the optical spectra, using the molar extinction coefficients $\varepsilon_{2800} = 42$ L mol⁻¹ cm⁻¹ for borosilicates and 155 L mol⁻¹ cm⁻¹ for SiO_2, respectively, as reported in Ref. [38].

echoes. The shear modulus G, bulk modulus K and elastic modulus E as well as the Poisson ratio ν were calculated using the following relations, which are applicable for isotropic materials [39]:

$$G = \rho \cdot c_T{}^2 \tag{1}$$

$$K = \rho \left(c_L{}^2 - \frac{4}{3} c_T{}^2 \right) \tag{2}$$

$$E = \rho \left[\frac{3c_L{}^2 - 4c_T{}^2}{(c_L/c_T)^2 - 1} \right] \tag{3}$$

$$\nu = \frac{c_L{}^2 - 2c_T{}^2}{2(c_L{}^2 - c_L{}^2)}. \tag{4}$$

2.3. Nanoindentation

Nanomechanical properties were characterized with a nanoindenter (G200, Agilent Inc.), equipped with a three-sided Berkovich diamond tip and a continuous stiffness measurement (CSM) option. Depth profiles of hardness H and elastic modulus E were obtained by applying a weak oscillation ($\Delta h = 2$ nm, $f = 45$ Hz) to the indenter tip [35]. On each glass specimen, 15 indents with a depth of 2 μm were generated at a constant strain-rate of $\dot{\varepsilon} = 0.05$ s^{-1}. The resulting load–displacement curves were analyzed using the Oliver and Pharr method [40], where H is defined as the load P divided by the projected contact area of the indenter tip A_c:

$$H = \frac{P}{A_c}. \tag{5}$$

The elastic modulus E was derived from the combined elastic response of the tested material and the diamond indenter ($E_i = 1141$ GPa, $\nu_i = 0.07$) by means of the following equation:

$$E = \left(1 - \nu^2\right) \left[\frac{1}{E_r} - \frac{1 - \nu_i{}^2}{E_i} \right]^{-1}, \tag{6}$$

with the reduced elastic modulus E_r,

$$E_r = \frac{S}{2} \sqrt{\frac{\pi}{A_c}}. \tag{7}$$

The symbol S represents the contact stiffness of the material and corresponds to the initial slope of the load–displacement curve upon unloading. The contact area used in Eqs. (5) and (7) was determined prior to the measurements by calibration of the Berkovich diamond tip on a fused silica reference glass sample (Corning 7980, Corning Inc.).

The indentation creep behavior was studied using a nanoindentation strain-rate jump test, as introduced by Maier et al. [41] and transferred for application on glasses by us in a previous study [35]. In this test, a three-sided Berkovich diamond tip penetrates the glass surface at a constant strain-rate of 0.05 s^{-1} down to 500 nm. During further penetration into the material, the strain-rate is changed every 250 nm, and the alteration of the hardness is determined with the CSM equipment ($\Delta h = 5$ nm, $f = 45$ Hz). On every glass specimen, 10 such tests with strain-rates of 0.05; 0.007 and 0.001 s^{-1} were performed. With the assumption of a depth-independent hardness ($\dot{H}/H = 0$) the applied strain-rate, defined as the loading rate divided by the actual load $\dot{P}/P$, can be translated into the indentation strain-rate $\dot{\varepsilon}_i$ by [42]:

$$\dot{\varepsilon}_i = \frac{\dot{h}}{h} = \frac{1}{2} \left(\frac{\dot{P}}{P} - \frac{\dot{H}}{H} \right) = \frac{P}{2\dot{P}} = \frac{1}{2} \dot{\varepsilon}, \tag{8}$$

where the parameter $\dot{h}/h$ represents the indentation rate divided by the actual displacement of the indenter. Subsequently, the logarithm of the hardness ln$H$ can be plotted against the logarithm of the indentation strain-rate ln$\dot{\varepsilon}_i$ and the strain-rate sensitivity m can be derived from the slope of the linear regression curve [43,44]:

$$m = \frac{\partial \ln H}{\partial \ln \dot{\varepsilon}_i}. \tag{9}$$

An increase in the strain-rate sensitivity can be treated as the transition from a rigid-perfectly plastic material with $m = 0$ to an ideal Newtonian viscous solid with $m = 1$ [45,46].

2.4. Microindentation

The Vickers hardness H_V was determined using a microhardness tester (Duramin-1, Struers GmbH). On each specimen, 15 indents with a maximum load of 981 mN ($= 100$ g) were generated. The loading duration and dwell time were set to 15 s and 10 s, respectively. The residual imprints were subsequently analyzed with an optical microscope (AxioLab A1, Carl Zeiss Microscopy GmbH) and H_V was calculated from the following equation:

$$H_V = 1.8544 \frac{P}{d^2}, \tag{10}$$

where d stands for the length of the projected indent diagonals.

The crack resistance CR was approximated via Vickers indentation tests, according to Kato et al. [47]. For this purpose, the glass specimens were indented with stepwise increasing loads, and the amount of radial cracks emanating from the corners of the residual imprints were counted. From this, the probability of crack initiation PCI was derived as the ratio between the number of corners where a radial crack was formed and the total number of corners on all indents. The crack resistance is defined as the load at which an average of two cracks ($PCI = 50\%$) occurred. The probability of crack initiation was determined for loads between 49.05 mN ($= 5$ g) and 19.62 N ($= 2$ kg). Indents with small loads up to 981 mN were generated in the nanoindenter. For higher loads, the microhardness tester was used. On every specimen, at least 25 indents with loading durations of 25s and dwell times if 10s were generated.

The topography of the residual Vickers hardness imprints was analyzed using an Atomic Force Microscope (M5, Park Scientific Instruments), equipped with a MSCT microlever tip (Bruker Nano Analytics) with a specified tip radius of approximately 10 nm. All measurements were performed in contact mode. A calibration grid was measured before and after each run to validate the tip conditions. For the evaluation of the Vickers indents an area of 10×10 μm was scanned with a resolution of 0.25 Å and 0.025 Å in the lateral and vertical directions, respectively. Indents with a peak load of 100 mN were created initially using the nanoindenter as described above. After this, the indentation volume V_i^-, which forms below the specimen surface, as well as the pile-up volume V_i^+, which can be observed at the periphery of the indent, were determined from the AFM profile. Subsequently, the indented glass specimen was annealed for 2 h at a temperature of $T/T_g \sim 0.9$ and both the indentation volume, now V_a^-, and the pile-up volume, now V_a^+, were determined once again. During this thermal treatment, a part of the total compaction is recovered due to structural relaxation, yielding the actual densified volume V_d [48–51]. The contribution of

Table 2
Mechanical properties of glasses in the system Na$_2$O–B$_2$O$_3$–SiO$_2$: Shear modulus G, bulk modulus K, elastic modulus E, Poisson ratio v, hardness H, strain-rate sensitivity m, Vickers hardness H_V and crack resistance CR. LBS and KBS as well as the soda-lime silicate glass, NCS, are added for comparison. Data on v, E, H and m are taken from Ref. [35], except for 2N8B, KBS and Duran.

Glass	G (GPa)	K (GPa)	E (GPa)[b]	v	E (GPa)[c]	H (GPa)	m	H_V (GPa)	CR (N)
2N8B	17.8[a]	35.2[a]	45.8[a]	0.283[a]	41.3 ± 0.2	4.09 ± 0.03	0.0283	3.53 ± 0.20	3.30
NBS A	16.8 ± 0.1	30.6 ± 0.5	42.6 ± 0.7	0.268 ± 0.006	41.6 ± 0.2	3.96 ± 0.03	0.0259	3.58 ± 0.12	6.55
NBS B	13.3 ± 0.1	23.0 ± 0.3	33.5 ± 0.5	0.257 ± 0.005	32.1 ± 0.1	3.68 ± 0.03	0.0270	3.15 ± 0.15	12.16
NBS C	23.1 ± 0.2	36.5 ± 0.7	57.3 ± 1.0	0.238 ± 0.007	57.1 ± 0.2	5.33 ± 0.03	0.0279	5.35 ± 0.33	7.26
NBS D	18.6 ± 0.1	29.1 ± 0.5	46.0 ± 0.7	0.237 ± 0.005	44.4 ± 0.1	4.98 ± 0.03	0.0240	3.75 ± 0.18	6.83
NBS1	32.7 ± 0.2	44.4 ± 0.6	78.8 ± 1.0	0.204 ± 0.004	81.4 ± 0.3	7.26 ± 0.04	0.0211	6.20 ± 0.32	0.41
NBS2	23.0 ± 0.2	32.1 ± 0.6	55.7 ± 1.0	0.210 ± 0.006	50.6 ± 0.2	5.89 ± 0.04	0.0209	4.25 ± 0.22	3.44
Duran	26.7[a]	35.6[a]	64.0[a]	0.200[a]	61.9 ± 0.2	7.18 ± 0.03	0.0180	6.47 ± 0.28	4.41
BK7	32.5 ± 0.3	44.4 ± 0.9	78.4 ± 1.5	0.206 ± 0.007	84.4 ± 0.3	7.97 ± 0.05	0.0223	6.62 ± 0.26	0.20
LBS	23.9 ± 0.2	32.0 ± 0.6	57.5 ± 1.0	0.201 ± 0.006	56.7 ± 0.3	7.01 ± 0.07	0.0149	6.42 ± 0.34	2.14
KBS	26.3 ± 0.2	36.0 ± 0.6	63.5 ± 1.1	0.206 ± 0.005	64.0 ± 0.2	6.92 ± 0.03	0.0181	6.33 ± 0.29	6.49
NCS	28.9 ± 0.2	42.3 ± 0.8	70.7 ± 1.3	0.221 ± 0.007	76.0 ± 0.4	6.67 ± 0.04	0.0164	5.36 ± 0.27	1.09
SiO$_2$	29.9[a]	35.4[a]	70.0[a]	0.170[a]	71.6 ± 0.3	9.30 ± 0.12	0.0068	7.53 ± 0.51	–

[a] Elastic constants of 2N8B, Duran and SiO$_2$ were taken from Ref. [55] and the corresponding data sheets, respectively.
[b] Values of E were determined by ultrasonic echography.
[c] Values of E were determined by nanoindentation.

densification to the overall indentation deformation can finally be esti-mated from the temperature-induced volume recovery V_R, [49]

$$V_R = \frac{V_d}{V_i^-} = \frac{(V_i^- - V_a^-) + (V_a^+ - V_i^+)}{V_i^-}. \tag{11}$$

With the progressive penetration of the indenter tip into the glass sur-face a part of the material deformed by volume-conservative shear flow is pushed out of the indent, leading to pile-up along the edges of the resid-ual imprints [51,52]. The pile-up ratio V_P can therefore be regarded as an indicator for the shear-mediated deformation of the material [53]:

$$V_P = \frac{2V_i^+ - V_a^+}{V_i^-}. \tag{12}$$

3. Results

Experimental data on the physical and mechanical properties of the studied glasses are summarized in Table 2. The compositional depen-dence of some selected physical and mechanical properties in the sodium-borosilicate system is presented in Fig. 1. In a first consideration, the experimental results of T_g, ρ, E, v and H_V are in a good agreement with literature data. Only small variations can be seen between the values of E determined by ultrasonic echography and by nanoindentation. However, for all glass compositions tested, the values of H are higher than H_V. The origin of this lies in the large contribution of elastic deformation to the in-dentation response of glasses, which results in a discrepancy between the contact area under load and the size of the residual hardness imprint [54].

In the context of deformation behavior, sodium-borosilicate glasses are commonly referred-to as so-called anomalous glasses, where the plastic deformation is controlled by the compaction of the free volume inside the glass network. This argumentation is based on the observa-tion of ring and cone cracks around the indentation marks in vitreous SiO$_2$ and other commercially available glasses with high free volume and containing only small amounts of network modifiers, e.g., the Duran-type composition presented in Fig. 2a [53,71,95,105–107]. On the other hand, a pronounced contribution of volume-conservative shear flow to plastic deformation was observed for glasses with high modifier concentrations, e.g., BK7-type composition (Fig. 2b), or small values of K, e.g., NBS D (Fig. 2d) and NBS A (Fig. 2e) [34,68,71,108].

To obtain a systematic and clearer view at this classification, the influence of densification and shear-mediated plastic deformation was evaluated for the present series of sodium-borosilicate glasses. Data on the as-obtained indentation volume V_i^- and pile-up volume V_i^+, and on the post-annealing volumes V_a^- and V_a^+, the resulting volume recovery

V_R and the pile-up ratio V_P of two technical glasses (Duran, BK7) as well as three model glasses (NBS A, C, D) are summarized in Table 3. Values for sodium borate [72] and vitreous silica [49,53] can be found in the literature.

In Fig. 3 the probability for the formation of radial cracks PCI is shown for the glasses investigated in the current study. With increasing load, the values of PCI increase for all glass compositions tested, but the onset for the initiation of the first radial crack differs significantly. In order to get some information on the compositional dependence of the radial crack initiation, the experimental data was fit to a sigmoidal function of the form $y = A_2 + (A_1 - A_2) / [1 + (x / x_0)^p]$, where A_1, A_2, p as well as x_0 are fitting constants, and the crack resistance CR was derived from the load, at which an average of two radial cracks were formed.

4. Discussion

4.1. Physical and mechanical properties

The physical and mechanical properties of glasses in the sodium-borosilicate system are well known to exhibit a strong compositional de-pendence. It has been shown, e.g., by Inoue et al. [109] and Barlet et al. [76], that this dependence can be attributed to distinct structural changes within the glass network. Amorphous B$_2$O$_3$ consists of corner-sharing BØ$_3$ triangles for which a major fraction (40–80%) is arranged in three-membered boroxol rings (B$_3$O$_6$)[1] [110–113]. The incorporation of a small amount of network modifier oxides, such as Na$_2$O, initially converts neutral BØ$_3$ units into charged [BØ$_4$]$^-$ tetrahedral units (see Fig. 1a) [10, 114], which results in a continuous increase of ρ [55,56,72,76], but also of the network connectivity up to a maximum at $R = 0.2$. The latter rep-resents the line of the boron oxide anomaly [32,34]. As a consequence, T_g [57,58,62,72], E [55,90,91,115] and H_V [72,90] increase as well. With the further addition of Na$_2$O ($R > 0.2$) the network connectivity starts to de-crease due to the formation of BO$_3$ units containing non-bridging oxygen ions, such as (BØ$_2$O)$^-$, (BØO$_2$)$^{2-}$ and (BO$_3$)$^{3-}$ [33,34]. However, this ef-fect is initially counterbalanced by the progressive conversion of addition-al BØ$_3$ units into [BØ$_4$]$^-$ tetrahedra, until a sudden decrease in the mechanical stability of binary sodium borate glasses can be observed for values exceeding $R > 0.5$, where the formation of non-bridging oxygen ions becomes detectable by NMR spectroscopy [36,116].

Referring to the ternary system, sodium-borosilicate glasses with low concentrations of Na$_2$O ($R \leq 0.5$) can be treated as a binary sodium borate glass diluted by SiO$_2$ [36,116,117]. SiO$_2$ builds-up a network of

---

[1] For ring member classification the nomenclature of silicate glasses is employed, which counts the number of SiO$_4$-tetrahedra or network forming polyhedra per ring, not the no-menclature commonly used in borate chemistry, in which the number of participating atoms per ring unit is counted, e.g., six-membered ring for boroxol.
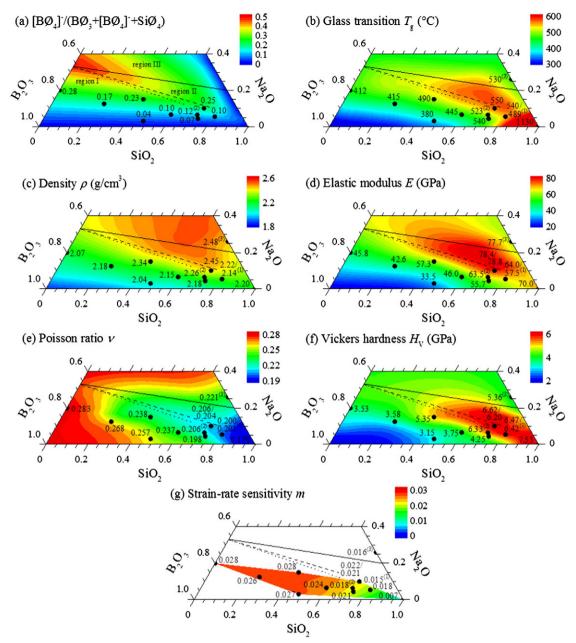
Fig. 1. Structural, physical and mechanical properties of glasses in the system Na_2O–B_2O_3–SiO_2: (a) Fraction of $[BØ_4]^-$ units per network former $[BØ_4]^-/(BØ_3 + [BØ_4]^- + SiØ_4)$, according to Ref. [56], (b) glass transition T_g, (c) density ρ, (d) elastic modulus E, (e) Poisson ratio ν, (f) Vickers hardness H_V and (g) strain-rate sensitivity m. The ternary contour diagrams of T_g [33–35,53,57–74], ρ [33–35,53,55,56,64–73,75–88], E [53,55,67–71,77–83,86–95], ν [35,53,55,67–69,79–83,86–89], H_V [31,53,68–73,84–86,95–104] and m [35] are derived from inter- and extrapolation of experimental results from the current study and literature data from previous studies. The black dots represent the glass compositions investigated in this work, where minor amounts of Al_2O_3 or other network modifier oxides (e.g. Li_2O, K_2O) are treated as B_2O_3 and Na_2O, respectively. In total, the contour diagrams result from (b) 226, (c) 184, (d) 127, (e) 77, (f) 97 and (g) 10 data points, respectively. Data of LBS (1) and KBS (2) as well as of the soda-lime silicate glass, NCS (3) are also shown for comparison. Drawn lines correspond to the different glass-forming regions, as proposed by Yun and Bray [36], region I: $0.5 \leq R$ (dotted line), $0.5 < R < R_{max} = 0.5 + 0.0625K$ (dashed line), region II: $R_{max} < R < R_1 = 0.5 + 0.25K$ (solid line) and region III: $R_1 < R < R_2 = 1.5 + 0.75K$. $R = Na_2O/B_2O_3$ and $K = SiO_2/B_2O_3$.

fully polymerized interconnected $SiØ_4$ tetrahedra, where the presence of Na_2O converts $BØ_3$ triangles into $[BØ_4]^-$ tetrahedra [36,116,117]. Within this region T_g [61–67,109], ρ [56,64–67,85,87,109], E [67,87,109], and H_V [85,87,98,99] increase, while ν decreases [67], regardless of whether B_2O_3 is substituted by Na_2O (increasing R) or SiO_2 (increasing K). On the other hand, the indentation creep response seems to be affected primarily by the amount of SiO_2 inside the glass network. With increasing SiO_2 concentration at the expense of Na_2O and B_2O_3, respectively, the network dimensionality increases [56,76] and associated with this the values of m continuously decrease from 0.0283 for sodium borate down to 0.0067 for vitreous silica. This result is in accordance with our previous findings on the indentation creep response of glasses with small Poisson

ratios up to $\nu \sim 0.33$, where a higher indentation creep resistance has been noticed for glasses with a low atomic packing density and a highly cross-linked network [35].

In contrast to binary sodium borate glasses, the maximum amount of Na_2O that can be introduced in the glass network, before NBO formation, depends not only on R but also on K. According to the NMR-based structural model for sodium-borosilicate glasses proposed by Yun and Bray [36], the $[BØ_4]^-$ tetrahedra are initially present in the form of tetraborate and diborate groups. With the progressive incorporation of Na_2O, diborate groups are created at the expense of tetraborate groups. At $R = 0.5$, only diborate groups exist (Fig. 1, dotted lines). For values of $R > 0.5$ these diborate groups are converted into loose $[BØ_4]^-$ units,
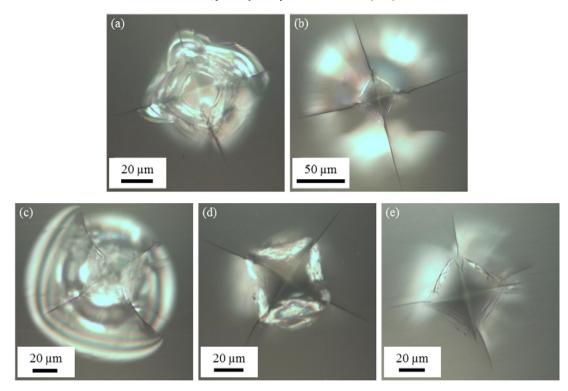
Fig. 2. Optical micrographs of the characteristic crack pattern formed by a Vickers indenter at a peak load of 9.81 N: (a) Duran, (b) BK7, (c) NBS2, (d) NBS D and (e) NBS A.

which allegedly bind to four $SiØ_4$ tetrahedra on the one hand to create reedmergnerite-like groups $[BSi_3Ø_8]^-$ [36,116]. On the other hand danburite-like groups $[B_2Si_2Ø_8]^{2-}$ can form, which consist of two $[BØ_4]^-$ units connected to two $SiØ_4$ tetrahedra [118,119]. At $R_{max} = 0.5 + 0.0625K$, when all $SiØ_4$ tetrahedra are consumed by this process, the upper limit of the glass-forming region I (Fig. 1, dashed lines) is reached. In the glass-forming region II, additional Na_2O is shared between the borate and silicate networks, which leads to the formation of non-bridging oxygen ions at the $SiØ_4$ tetrahedra [36,116]. As a consequence of the decreasing connectivity in the silicate network ν increases and T_g [59–62,64–66,68], E [68,78,109] as well as H_V [68,85,98] exhibit a maximum in the region in-between R_{max} and $R_1 = 0.5 + 0.25K$ (Fig. 1, solid lines). Afterwards, within the subsequent glass-forming region III, the mechanical properties decrease significantly due to the formation of non-bridging oxygen ions in both the borate and silicate networks [116]. On the contrary, ρ still increases slightly with the replacement of the light boron atoms by the heavier sodium ion, and the molar volume decreases as the large voids in the loosely packed silica network are filled by the modifier cations [56,85,109].

Based on the structural models of Yun and Bray [36] as well as Budhwani and Feller [56], several authors tried to calculate the physical and mechanical properties of glasses in the system $Na_2O–B_2O_3–SiO_2$, such as T_g, ρ, E or H_V [56,76,109,120]. However, the application of this model remains still questionable. It has been shown, for example, that for glasses with $R > 0.5$ the silicate network is less depolymerized than predicted. Consequently, a substantially larger amount of non-bridging oxygen ions is attached to the borate network [34,76,116]. Another point to note is the discrepancy between the glass compositions with the minimum values of ν on the one hand and the maximum values of T_g, E and H_V on the other hand. Makishima and Mackenzie [121] and later on Rouxel [6] have demonstrated that glasses with a high degree of cross-linking and a low atomic packing density (e.g. vitreous silica) are usually associated with small values of ν, while glasses with a lower network connectivity and a higher atomic packing density (e.g. chalcogenide or metallic glasses) exhibit large values of ν. In binary sodium borate glasses ρ increases with increasing Na_2O concentration, even for $R > 0.5$ [55,56]. Nonetheless, with the addition of Na_2O, ν initially decreases, exhibits a minimum at around $R = 0.5$ and then re-increases for $R > 0.5$ [55]. This result indicates that the changes in ν can be primarily attributed to the increased connectivity in the glass network. A similar behavior is observed in the ternary sodium-borosilicate glass system. Here, ρ continuously increases

Table 3
Indentation volume analyses of glasses in the system $Na_2O–B_2O_3–SiO_2$. The diagonal length d, indentation depth h, indentation volume V^- and pile-up volume V^+ of Vickers indents with a peak load of 100 mN as determined from AFM analyses are given. Subscripts "i" and "a" indicate the corresponding volumes prior to and after a thermal treatment for 2 h at $T/T_g = 0.9$, respectively. For comparison, values for 2N8B [72] and SiO_2 as taken from Ref. [49] are also reported. The parameters V_R and V_P represent the indentation volume recovery and the pile-up ratio, respectively.

Glass	Before annealing				After annealing				Recovery	
	d_i (µm)	h_i (nm)	V_i^- (µm³)	V_i^+ (µm³)	d_a (µm)	h_a (nm)	V_a^- (µm³)	V_a^+ (µm³)	V_R (%)	V_P (%)
2N8B[a]	10.89 ± 0.07	0.895 ± 0.009	8.300 ± 0.020	0.270 ± 0.020	10.13 ± 0.07	0.574 ± 0.004	2.260 ± 0.040	0.530 ± 0.040	75.9 ± 0.9	0.1
NBS A	7.51 ± 0.01	0.569 ± 0.003	2.759 ± 0.008	0.035 ± 0.002	6.66 ± 0.06	0.381 ± 0.016	1.204 ± 0.147	0.030 ± 0.009	56.2 ± 6.2	1.4 ± 0.5
NBS C	6.12 ± 0.06	0.464 ± 0.004	1.502 ± 0.018	0.025 ± 0.011	5.64 ± 0.06	0.307 ± 0.012	0.470 ± 0.012	0.039 ± 0.004	69.6 ± 3.8	0.7 ± 0.4
NBS D	7.21 ± 0.14	0.486 ± 0.017	1.904 ± 0.088	0.028 ± 0.010	6.10 ± 0.10	0.258 ± 0.023	0.416 ± 0.025	0.034 ± 0.005	78.5 ± 10.3	1.2 ± 0.7
Duran	5.12 ± 0.09	0.445 ± 0.010	1.097 ± 0.023	0.031 ± 0.007	4.53 ± 0.03	0.221 ± 0.020	0.376 ± 0.013	0.038 ± 0.003	66.4 ± 5.6	2.2 ± 0.8
BK7	5.20 ± 0.07	0.463 ± 0.005	1.176 ± 0.031	0.067 ± 0.003	4.94 ± 0.03	0.276 ± 0.006	0.594 ± 0.016	0.022 ± 0.006	45.7 ± 6.0	8.0 ± 3.5
SiO_2	5.16 ± 0.10	0.420 ± 0.025	1.030 ± 0.031	0.020 ± 0.006	4.08 ± 0.15	0.230 ± 0.014	0.200 ± 0.014	0.140 ± 0.025	92.2 ± 4.0	–

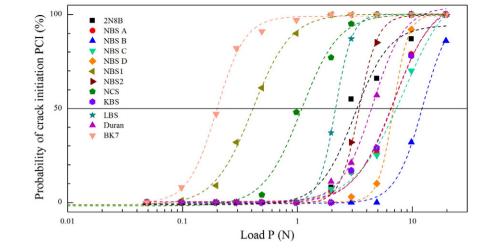[a] Values were determined for Vickers indents with a peak load of 245 mN.

Fig. 3. Probability of radial crack formation *PCI* as a function of applied Vickers indentation load *P* for glasses investigated in the current study. The experimental data was fit to a sigmoidal function of the form $y = A_2 + (A_1 - A_2) / [1 + (x / x_0)^p]$ (dashed lines), and the crack resistance (solid line) was derived from the load at which an average of two radial cracks (*PCI* = 50%) formed at the corners of the residual Vickers hardness imprints.

with increasing *R* and *K*, while ν initially decreases until it reaches a certain minimum in a small compositional region that coincides with $0.5 \leq R \leq 0.5 + 0.0625K$. The following re-increase of ν can most likely be attributed to the incipient depolymerization of the glass network. Although contradictory to the early NMR-based structural model for sodium-borosilicate glasses, this assumption receives support from various studies in which the presence of non-bridging oxygen ions in the borate [34,76,117] and silicate networks [5,34,85], respectively, was verified.

4.2. Indentation deformation

Compared to their (hypothetic or real) crystalline analogues, glass networks exhibit a higher degree of free volume, which results in a notable degree of compressibility. In the case of vitreous silica, the application of high hydrostatic pressure can lead to an increase of the density by as much as 20% [122–124]. This behavior was confirmed for other types of glasses as well, including vitreous boron oxide [125–127], alkali–alkaline earth borates [128–130] or sodium-borosilicate glasses [13, 17,128]. The ability of a glass to densify under pressure depends mainly on the atomic packing density C_g, which is defined as the ratio between

the theoretical molar volume occupied by the ions and the effective molar volume of the glass [6]:

$$C_g = \rho \frac{\sum f_i V_i}{\sum f_i M_i}. \tag{13}$$

In the above equation $V_i = 4/3\pi N(x r_A^3 + y r_B^3)$ represents the molar volume of an oxide $A_x B_y$ with the molar fraction f_i and the molar mass M_i and the symbol N denotes the Avogadro number. The ionic radii r_A and r_B of the corresponding cations and anions, respectively, can be found in the literature [131].

Besides atomic packing density, a correlation between compressibility and the Poisson ratio has been established, as glasses with a more open network structure and small values of ν (such as vitreous silica) can be densified to a higher extent than close-packed structures with large values of ν, e.g., chalcogenide or metallic glasses [132]. A similar behavior was found for the indentation response of glasses [49,133, 134]. Therefore, in Fig. 4 the values of V_R determined for the present series of sodium-borosilicate glasses are shown as a function of ν and C_g, together with results from earlier studies on glasses in this system [68, 69,72]. In addition, literature values from other glass systems, mostly
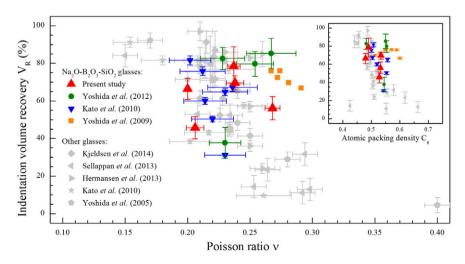

Fig. 4. Correlation between the indentation volume recovery V_R of glasses and the Poisson ratio ν. The inset shows V_R as a function of the atomic packing density C_g.

aluminosilicate and alkali–alkaline earth silicate glasses, were added for comparison [47,49,53,79,135,136]. Values from Refs. [47,68] were included using the approximation that V_R is linked to the recovery of indentation depth D_R by the simple relationship $D_R = 2.4V_R$ [53].

At a first glance, the contribution of densification to the indentation deformation decreases with increasing ν or increasing C_g (see inset in Fig. 4), which agrees quite well with the previously observed trend described above. However, within the range of $0.2 \leq \nu \leq 0.3$, where almost all sodium-borosilicate glasses are located, marked differences in V_R are observed for similar values of ν. In contrast, little or no changes of V_R are found even for large variations in ν for other glasses. Interestingly, the same observations were made for the dependency of V_R on C_g. These results imply a significant influence of additional parameters on the indentation-induced densification of glasses besides the atomic packing density and the elastic properties of the material. In earlier studies, distinct alterations in the indentation deformation behavior were reported depending on the experimental conditions, such as the maximum load or the geometry of the indenter tip [50–52,134, 137–139]. Usually, blunter indenter tips (e.g. spheres) promote densification, while the high stress concentration below sharp indenter tips (e.g. Berkovich, Vickers) facilitates the activation of shear flow in the material [134,138,139]. Another important aspect, which is not considered in the above analysis, is the alteration of the resistance against elastic–plastic deformation within the densified area under the indenter tip, as a result of changes in v, E and H_V, which might affect the further penetration of the indenter into the glass surface [17,128,130,133,140].

Despite the obvious experimental limitations of this method, a strong compositional dependence of V_R has been reported for aluminosilicate as well as alkali–alkaline earth silicate glasses [79,135,136]. Similarly, such a compositional dependence is confirmed also for the present system of Na_2O–B_2O_3–SiO_2, presented in Fig. 5. Although the available data in this system is rather limited, a local maximum of V_R is clearly visible for SiO_2-rich glasses and pure SiO_2 in particular [49,53,68,69]. These findings are quite consistent with the observations made, e.g., on alkali–alkaline earth silicate glasses [49,79]. They indicate that the SiO_2 sub-network governs the densification of SiO_2-rich sodium-borosilicate glasses. This is basically achieved by an increasing amount of smaller three- and four-membered silicate rings at the expense of larger five- and six-membered silicate rings, as well as by a decrease of the Si–O–Si bond angle [33,34,141,142]. However, increasing the atomic packing density by adding B_2O_3 or Na_2O to the glass, or creating non-bridging oxygen ions results in a continuous decrease of V_R and the transition from densification-controlled towards shear-mediated indentation deformation, where the minimum values of V_R are located in a narrow compositional range which corresponds to the region of maximum T_g, E or H_v and minimum ν, as shown in Fig. 1 in Section 3. At first view, this result is in contradiction to previous studies in which decreasing V_R with increasing ν has been reported [49,53,79]. Recalling the NMR-based structural model of Yun and Bray [36], the incorporation of Na_2O initially converts $BØ_3$ triangles into $[BØ_4]^-$ tetrahedra [36,116,117]. For $R > 0.5$, the $[BØ_4]^-$ tetrahedra were expected to be linked to the $SiØ_4$ tetrahedra

and form either reedmergnerite $[BSi_3Ø_8]^-$ or danburite $[B_2Si_2Ø_8]^{2-}$-type structural units [118,119], which seem to impede the densification of the silicate sub-network. However, very recent thermodynamic considerations have demonstrated that these borosilicate ring structures do not form spontaneously when the Na_2O to B_2O_3 ratio exceeds a value of 0.5. Instead, the connectivity between the silicate and borate sub-networks increases continuously as the Na_2O and B_2O_3 concentrations increase (see Fig. 3b) [143], while at the same time, the ability of the glass to densify decreases. Furthermore, a prevalent signal due to B_3–O–Si bonds was verified in a Pyrex-type glass by 2D NMR, with no evidence for preferential B_4–O–Si bonding, despite the high N_4 ratio in this glass composition [144]. With respect to these NMR results, some of the assumptions on which the empirical structural models are based, need to be reconsidered carefully.

Besides the SiO_2-rich region, a second local maximum of V_R can be seen within the B_2O_3-rich region. The large contribution of densification to the indentation deformation of B_2O_3-containing glasses can be attributed to structural alterations in the B_2O_3 sub-network. High-pressure studies on amorphous B_2O_3 [145–147] as well as borate glasses [129,148] revealed that the densification of B_2O_3-containing glasses is based on the breakage of three-membered boroxol rings during loading and the conversion of $BØ_3$ units into temporarily over-coordinated $[BØ_4]^-$ groups. Although this over-coordination of boron is released after unloading, only a small fraction of the previously existing boroxol rings is restored and a permanent densification is achieved as a consequence of the reduced free volume inside the glass network [147,149]. Nonetheless, in borate glasses with minor amounts of network modifier oxides, such as Na_2O, a slightly reduced contribution of densification to the indentation deformation has been noticed in comparison to glasses with larger amounts of Na_2O [72]. It has been suggested that this effect originates from the simultaneous activation of a shear flow mechanism, which is thought to proceed over a sliding motion of the planar boroxol rings [72,150]. Since the fraction of boroxol rings decreases continuously with increasing Na_2O concentration [143], the influence of the corresponding shear and densification mechanisms diminishes. At the same time, the densification mechanism was found to shift towards a change in the statistics of borate rings containing at least one $[BØ_4]^-$ group [33,72]. For that reason an initial increase in V_R can be observed with increasing Na_2O concentration, until the creation of non-bridging oxygen ions facilitates plastic deformation through localized shear flow [72]. It is therefore not unexpected that the high contribution of densification in the B_2O_3-rich region is found for glass compositions with Na_2O/B_2O_3 ratios at exactly the cross-over where the first non-bridging oxygen ions start to form, $R = 0.2$ [33,34], and at the resolution limit for the detection of non-bridging oxygen ions by NMR, $R = 0.5$ [36,116], respectively.

4.3. Crack initiation

With the progressive penetration of an indenter tip into a glass surface the stresses are initially accommodated by elastic–plastic deformation, visible in a residual hardness imprint [151]. However, at
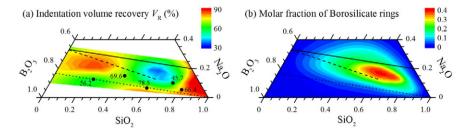

Fig. 5. (a) Compositional dependence of the indentation volume recovery V_R of glasses in the system Na_2O–B_2O_3–SiO_2. Black dots represent the glass compositions investigated in the current study. Lines drawn correspond to constant Na_2O/B_2O_3 ratios of $R = 0.2$ (dotted line), $R = 0.5$ (dashed line) and $R = 0.5 + 0.25K$ (solid line), with $K = SiO_2/B_2O_3$. The ternary contour diagram is build up of 25 data points. (b) Molar fraction of four-membered borosilicate rings, reedmergnerite $[BSi_3Ø_8]^-$ and danburite $[B_2Si_2Ø_8]^{2-}$-type structural units, according to Ref. [143].

sufficiently high loads the mismatch between the plastically deformed volume, which is assumed to be restricted to a hemispherical area below the indenter tip, and the adjacent elastically deformed material can cause the formation of ring, median, radial, or lateral cracks [107]. By analyzing the stress fields around the indented region, Yoffe [134] developed a model which has been applied successfully for the description of the differences in the crack initiation behavior for a variety of glasses [53,107,139]. In Yoffe's model, the elastic stress field of a point load P normal to the surface of a semi-infinite half-space can be described by the combination of a Boussinesq stress field with the spherical polar coordinates r, θ and ϕ, and a blister field. The corresponding stress components σ of this field are re-written from [134],

$$\sigma_{rr} = \frac{P}{2\pi r^2}\left[1-2\nu-2(2-\nu)\cos^2\theta\right] + \frac{4B}{r^3}\left[(5-\nu)\cos^2\theta - (2-\nu)\right] \quad (14)$$

$$\sigma_{\theta\theta} = \frac{P}{2\pi r^2}\frac{(1-2\nu)\cos\theta}{(1+\cos\theta)} - \frac{2B}{r^3}(1-2\nu)\cos^2\theta \quad (15)$$

$$\sigma_{\phi\phi} = \frac{P}{2\pi r^2}(1-2\nu)\left[\cos\theta - \frac{1}{1+\cos\theta}\right] + \frac{2B}{r^3}(1-2\nu)\left(2-3\cos^2\theta\right) \quad (16)$$

$$\sigma_{r\theta} = \frac{P}{2\pi r^2}\frac{(1-2\nu)\sin\theta\cos\theta}{(1+\cos\theta)} + \frac{4B}{r^3}(1+\nu)\sin\theta\cos\theta \quad (17)$$

$$\sigma_{r\phi} = \sigma_{\theta\phi} = 0, \quad (18)$$

where the first term describes the Boussinesq stress field around a conical indenter tip with the radius r and the half-included angle ψ. In particular, Yoffe's model can also be used to estimate the elastic stress fields around pyramidal indenter tips, since the contact stresses induced by both tip geometries are the same [152]. Moreover, the shape of a Vickers indenter with $\psi = 68°$ can be approximated by an equivalent conical indenter with $\psi = 70.3°$, which implies that the corresponding conical indenter has the same projected contact area ($A_c = \pi r^2$) as the Vickers indenter ($A_c = 2a^2$) [153]. As a consequence, the term πr^2 in Eqs. (14)–(17) can be replaced by $2a^2$, where a is one half of the indentation diagonal d. If the hardness is load-independent, $P/2a^2$ may be substituted by H [53].

The second term in Yoffe's stress field analysis represents the blister field, which accounts for the free surface created by densification and shear-mediated change of the shape and volume of the previously undeformed material. Here the parameter B is a measure of the strength of the blister field. For a Vickers indenter, B can be determined from the indentation topography by the following equation [53]:

$$B = \frac{Ea^3}{2\pi(1+\nu)(1-2\nu)\tan\psi}(1-V_R-V_P). \quad (19)$$

Based on these considerations the elastic stress field around a Vickers indenter can be calculated and the driving force for the initiation of ring $\sigma_{rr}(r=a, \theta=\pi/2)$, median $\sigma_{\theta\theta}(r=a, \theta=0)$, radial $\sigma_{\phi\phi}(r=a, \theta=\pi/2)$ and lateral cracks $\sigma_{rr}(r=a, \theta=0)$ can be estimated, according to Sellappan et al. [53], by:

$$\sigma_{rr}(r=a,\ \theta=\pi/2)/H = \frac{1-2\nu}{2} + \frac{2(\nu-2)(1-V_R-V_P)}{\pi(1+\nu)(1-2\nu)\tan\psi}\left(\frac{E}{H}\right) \quad (20)$$

$$\sigma_{\theta\theta}(r=a,\ \theta=0)/H = \frac{1-2\nu}{4} - \frac{(1-V_R-V_P)}{\pi(1+\nu)\tan\psi}\left(\frac{E}{H}\right) \quad (21)$$

$$\sigma_{\phi\phi}(r=a,\ \theta=\pi/2)/H = \frac{2\nu-1}{2} + \frac{2(1-V_R-V_P)}{\pi(1+\nu)\tan\psi}\left(\frac{E}{H}\right) \quad (22)$$

$$\sigma_{rr}(r=a,\ \theta=0)/H = -\frac{3}{2} + \frac{6(1-V_R-V_P)}{\pi(1+\nu)(1-2\nu)\tan\psi}\left(\frac{E}{H}\right), \quad (23)$$

where all stress components are normalized to H. It has to be noted that the above equations were developed for the stresses, which occur during loading at the maximum load P. Therefore, systematic differences occur in crack initiation as predicted by such a stress field analysis, and as experimentally observed on crack patterns (which typically occur after unloading): a substantial fraction of cracking occurs during unloading rather than during loading [107,154,155]. In addition, other effects, which have a significant influence on the indentation deformation and defect resistance, such as the indentation size effect [156], the load-dependence of V_R [50,137,138], or the presence of atmospheric moisture [107,157], are not considered in Yoffe's model.

The initiation of cracks is driven by the presence of tensile stresses, which continuously decrease in intensity with increasing distance from the center of pressure r. Since the stresses within the plastically deformed area are compressive, the highest tensile stresses can be expected at the region between the plastically deformed volume below the indenter tip and the surrounding elastically deformed material, at $r = a$ [134]. However, the exact position of the tensile stress maximum depends significantly on B. Eq. (19) indicates that this value is mainly controlled by the term $(1 - V_R - V_P)$, whereas the magnitude of this parameter continuously decreases as the contribution of densification on the indentation deformation increases [53]. The application of ν as an indicator for the densification and shear-mediated deformation of glasses was discussed in the previous section. Contrary to alkali–alkaline earth silicate glasses [79,135,136], ν is not a suitable parameter for the description of the indentation deformation behavior of sodium-borosilicate glasses, as seen from Fig. 5. Nonetheless, ν has become a useful parameter for the comparison of crack formation in different glass systems [53]. For this reason, the elastic stresses around a Vickers indenter estimated for the present series of sodium-borosilicate glasses are shown in Fig. 6 as a function of ν, together with literature values from Refs. [49,53].

To obtain insights on the influence of the glass composition on the elastic stress fields in the system $Na_2O–B_2O_3–SiO_2$, the further discussion will focus on the technical glasses with Duran- and BK7-type compositions, as well as one glass series with compositions along boron oxide anomaly ($R = 0.2$), at which distinct changes in the glass properties have been reported previously [5,55,158]. Starting at $B = 0$, or $(1 - V_R - V_P) = 0$ (inset in Fig. 6), and for small values of ν, the tensile stresses exhibit a maximum at the surface $\sigma_{rr}(r=a, \theta=\pi/2)$ and the initiation of ring cracks occurs during loading [134]. This result is consistent with the observation of ring and cone cracks in so-called anomalous glasses (e.g. vitreous silica), which are known to deform mainly by compaction of the free volume inside their glass network [31,107,159]. The magnitude $(1 - V_R - V_P)$ and the stresses at the surface decrease rapidly with higher contribution of volume-conservative shear flow on the indentation deformation, while the sub-surface tensile stresses along the indenter axis $\sigma_{\theta\theta}(r=a, \theta=0)$ diminish only slightly. As a consequence, median cracks form below the indenter tip during loading in addition to the previously mentioned ring cracks [134]. During unloading these circular cracks expand towards the surface and appear as half-penny shaped cracks [107,160]. At sufficiently high loads, lateral and radial cracks may occur, but these cracks remain relatively short since their propagation is confined by the presence of ring and cone cracks, as can be seen for example in the optical micrograph of a residual Vickers hardness imprint in the Duran-type composition in Fig. 2a in Section 3.

Moving from the Duran- to the BK7-type composition (Fig. 2b), where a considerable amount of non-bridging oxygen ions has been verified by NMR and Raman spectroscopy [11,34], the contribution of densification to the indentation deformation becomes less pronounced and the magnitude of $(1 - V_R - V_P)$ increases. In the stress field analysis, such an effect is associated with a further decrease of the sub-surface tensile stresses along the indenter axis $\sigma_{\theta\theta}(r=a, \theta=0)$. However, at the same time the tensile stresses at the periphery of the indenter $\sigma_{\phi\phi}(r=a, \theta=\pi/2)$ increase and radial cracks start to emanate from
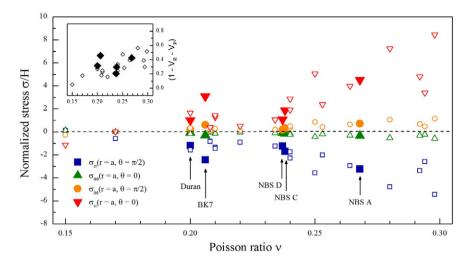
Fig. 6. Elastic stresses σ around Vickers indents in glasses as a function of the Poisson ratio ν. The stress components $\sigma_{rr}(r = a, \theta = \pi/2)$, $\sigma_{\theta\theta}(r = a, \theta = 0)$, $\sigma_{\phi\phi}(r = a, \theta = \pi/2)$ and $\sigma_{rr}(r = a, \theta = 0)$, normalized to the hardness H, represent the driving force for the initiation of ring, median, radial and lateral cracks, respectively. Filled symbols denote the glasses investigated in the current study and open symbols were taken from the literature [49,53]. In the inset, the parameter $(1 - V_R - V_P)$ is shown as a function of ν, where V_R and V_P denote indentation volume recovery and pile-up ratio, respectively.

the corners of the indent during loading. During unloading these cracks propagate further along the specimen surface, and the parallel initiation of additional tensile stresses below the indenter tip $\sigma_{rr}(r = a, \theta = 0)$ results in the formation of sub-surface lateral cracks [134]. This crack initiation behavior is typical for so-called normal glasses (e.g. soda-lime silicates), which – as a hypothesis – deform through shear-flow along weak ionically bonded interfaces in the network modifier-rich regions [31,52,107].

Based on these theoretical considerations, Sellappan et al. [53] evaluated the transition from ring and cone cracks via median to radial and lateral cracks and noticed a correlation with ν. On the one hand, ring/cone (subscript "C") and median cracks (subscript "M") can be expected for glasses with small values of ν, on the other hand radial (subscript "R") and lateral cracks (subscript "L") occur predominantly in glasses with higher values of ν. Depending on the elasto-plastic ratio E/H of the glass, the transition from cone and median to median and radial cracking, ν_{CM-MR} (~0.18), as well as the subsequent transition from median and radial to lateral and radial cracking, ν_{MR-LR} (~0.21), can shift to smaller values of ν, in the case of an increasing E/H ratio, or larger values of ν if the E/H ratio decreases.

The transition from an anomalous to a normal glass can also be demonstrated in the present series of sodium-borosilicate glasses, when the SiO$_2$ concentration decreases along the boron oxide anomaly from vitreous SiO$_2$ to NBS A. For high concentrations of SiO$_2$ and large values of $K = 3.57$ (NBS 2, Fig. 2c), the formation of ring and cone cracks is still visible, but with additional Na$_2$O and B$_2$O$_3$ (and the continuous decrease of K, NBS D: $K = 1.79$, Fig. 2d; NBS A: $K = 0.40$, Fig. 2e), ring and cone cracks gradually disappear. Simultaneously, the initiation of radial cracks and sub-surface lateral cracks was noticed, especially in the NBS A glass specimen. However, in contrast to the predictions from the stress field analyses, ring and cone cracks are still seen in the NBS D glass sample.

Although oxide glasses are termed as brittle materials, they can undergo distinct plastic deformation in the nano- and micrometer scales. The concept of brittleness is based on the relation between deformation and fracture [161]. Glasses with values of ν lower than ~0.31, such as SiO$_2$ or soda-lime silicates, exhibit only very small fracture energies. As a consequence, catastrophic failure occurs before a permanent plastic deformation can be achieved [162]. It is well known that the theoretical strength of brittle materials is reduced by the presence of small microscopic flaws or cracks. The resistance against the initiation and propagation of such defects, namely the toughness, is a crucial factor in technical exploitation of high-strength glasses [4,8].

In the previous section it has been shown, that the initiation of cracks in an indentation test can be attributed to elastic stresses, which originate from the mismatch between the plastically deformed volume and the surrounding elastically deformed material. Depending on the deformation mechanism and the elastic–plastic properties of the material, several different crack patterns can develop, but of practical importance are only median and radial cracks, since their propagation perpendicular to the glass surface is responsible for the fracture under bending or tensile loading conditions [95,106]. The resistance against the formation of median and radial cracks can be approximated by a pragmatic Vickers indentation test. In this test, the glass specimen is indented with stepwise increasing loads until the appearance of cracks can be observed at the corners of the residual hardness imprint [70]. In the current study, the sodium-borosilicate glasses were indented with loads ranging from ~50 mN up to ~20 N and the amounts of radial cracks emanating from the corners of the indent were counted using an optical microscope. On this basis, the crack resistance CR was derived from the load, at which an average of two radial cracks were formed. The results are shown in Fig. 7, together with literature values from Kato et al. [68]. Despite the limited number of data points, some distinct compositional trends are obvious. At first, CR seems to decrease with increasing Na$_2$O concentration, with the smallest values of CR corresponding to glass compositions with preferentially shear-mediated indentation deformation. This result is in good agreement with previous observations, in which an increasing resistance against radial crack formation with increasing contribution of densification to the indentation
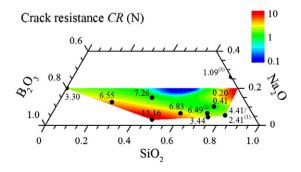

Fig. 7. Crack resistance CR of glasses in the system Na$_2$O–B$_2$O$_3$–SiO$_2$. Black dots represent the glass compositions investigated in the current study. LBS (1) and KBS (2), as well as the soda-lime silicate glass, NCS (3), were added for comparison. The contour diagram is build-up of 17 data points.

deformation was reported [53,68,107,139]. Additional support for these findings arises from the stress field analysis, where it has been demonstrated that the initiation of radial cracks is favored in glasses which deform through localized shear flow, while the residual stresses which are responsible for the formation of radial cracks are substantially reduced in glasses with a marked contribution of densification to the indentation deformation [134]. However, the highest values of CR do not coincide with the maximum values of V_R. In fact, maximum values of CR were obtained for sodium-borosilicate glasses with small amounts of Na_2O and less than 60 mol% SiO_2. In previous studies, large values of CR were attributed to the more open structure of borate networks containing a high amount of $BØ_3$ units, which facilitates the plastic deformation through densification and makes the borate network less rigid in comparison to $[BØ_4]^-$-rich glasses [68,130]. However, this argumentation is contradictory to the observations made by Yoshida et al. [72], as discussed in Subsection 4.2. Furthermore, with respect to this argument, the second local maximum of CR close to the binary $Na_2O–SiO_2$ glasses has to be highlighted (interestingly, both compositional regions fall in the compositional region corresponding to the miscibility gaps in the system $Na_2O–B_2O_3–SiO_2$ [32,143,163], but a discussion of the effect of phase separation on the mechanical properties of sodium-borosilicate glasses is out of the scope of this study).

5. Conclusions

A detailed picture of the physical and mechanical properties of glasses from the sodium-borosilicate ternary is obtained through combining new experimental data on low-alkali glasses, including some technical multi-component alkali-borosilicates, with an extensive literature review. It is demonstrated that physical properties such as the glass transition temperature T_g and the density ρ can be correlated with mechanical properties such as the elastic modulus E and the Vickers hardness H_v predominantly through the SiO_2 content and the fraction of $[BØ_4]^-$ tetrahedral units within the glass network. That is, for low alkali-borosilicate glasses, the addition of a small amount of network modifier oxides converts neutral $BØ_3$ groups into charged $[BØ_4]^-$ units, which is accompanied by the aforementioned property increase. However, when the Na_2O-to-B_2O_3 ratio, R, exceeds a value of $R = 0.2$, the boron oxide anomaly, the network connectivity starts to decrease due to the formation of non-bridging oxygen ions. This effect is initially counterbalanced by the progressive conversion of $BØ_3$ groups into $[BØ_4]^-$ units, until a sudden decrease in the thermal (T_g) and mechanical stability (E, H_V) can be observed, most notably for values of $R > 0.5$, where the presence of non-bridging oxygen ions is also verified by NMR spectroscopy.

The contribution of densification to indentation-induced deformation, expressed as the indentation volume recovery V_R, reaches a maximum for silica-rich glasses, where the densification is based on congruent compaction of the SiO_2 sub-network. In such glasses, permanent densification is achieved through a re-arrangement of large five- and six-membered rings into smaller three- and four-membered ring structures, as well as through a decrease of the average Si–O–Si bond angle. The incorporation of Na_2O and/or B_2O_3 reduces the silica sub-network's ability to compact of the silica sub-network. On the one hand, this is simply due to the increased atomic packing density. At high network modifier concentrations, on the other hand, the plastic deformation through localized shear flow is facilitated by the creation of non-bridging oxygen ions. Besides this, a strong correlation between densification and the interconnectivity between the silicate and borate sub-networks is noticed, where the formation of four-membered reedmergnerite $[BSi_3O_8]^-$ and danburite $[B_2Si_2O_8]^{2-}$-type ring structures and, therefore, higher connectivity between $SiØ_4$ groups and $[BØ_4]^-$ units seems to result in a reduced compaction capacity.

The above-mentioned correlations qualitatively hold also for the crack initiation behavior and the phenomenological crack resistance CR. In SiO_2-rich glasses, where the deformation is mainly based on

densification, ring and cone cracks are observed upon indentation, while the transition towards shear-mediated deformation occurs with increasing B_2O_3 concentration and/or with the formation of non-bridging oxygen species. This transition later manifests in the well-known change from ring and cone crack patterns via median cracks to a predominantly lateral and radial crack arrangement. Additional support for this is obtained from a consideration of the elastic stress fields which form around the indent, where it has previously been demonstrated that the contribution of densification to indentation-induced deformation leads to a reduction of tensile stresses in the surface plane, which are in turn responsible for the initiation of radial cracks. As a consequence, high values of CR are achieved in glasses where the indentation deformation is driven by compaction. This is in accordance with previous observations, which were made in other silicate glass systems, e.g., aluminosilicates or alkali–alkaline earth silicates.

In some contrast to the classical calculations of elastic stress fields, the appearance of cone cracks is still visible in glasses with relatively large amounts of Na_2O and B_2O_3. Most notably, the largest values of CR were obtained for glass compositions, which do not exhibit the highest values of V_R. All these findings indicate that the structural evolution, such as the conversion of $BØ_3$ groups into $[BØ_4]^-$ units, the formation of non-bridging oxygen ions or the connectivity between the silicate and borate sub-networks, play an important role on the physical and mechanical properties as well as the indentation deformation and crack initiation behavior, and that for the generation of a full picture of this complex glass system, these phenomena have to be treated equally and beyond the simplified consideration of congruent compaction and shear flow alone.

References

[1] A. Ellison, I.A. Cornejo, Int. J. Appl. Glass Sci. 1 (2010) 87–103.
[2] M.M. Smedskjaer, R.E. Youngman, J.C. Mauro, Appl. Phys. A-Mater. 116 (2014) 491–504.
[3] J.C. Mauro, FMATS 1, 2014.http://dx.doi.org/10.3389/fmats.2014.00020.
[4] L. Wondraczek, J.C. Mauro, J. Eckert, U. Kuhn, J. Horbach, J. Deubener, T. Rouxel, Adv. Mater. 23 (2011) 4578–4586.
[5] D. Ehrt, Glass Technol. 41 (2000) 182–185.
[6] T. Rouxel, J. Am. Ceram. Soc. 90 (2007) 3019–3039.
[7] L. Wondraczek, J.C. Mauro, J. Eur. Ceram. Soc. 29 (2009) 1227–1234.
[8] C.R. Kurkjian, P.K. Gupta, R.K. Brow, Int. J. Appl. Glass Sci. 1 (2010) 27–37.
[9] J.C. Mauro, C.S. Philip, D.J. Vaughn, M.S. Pambianchi, Int. J. Appl. Glass Sci. 5 (2014) 2–15.
[10] P.J. Bray, S.A. Feller, G.E. Jellison, Y.H. Yun, J. Non-Cryst, Solids 38–9 (1980) 93–98.
[11] D. Möncke, D. Ehrt, H. Eckert, V. Mertens, Phys. Chem. Glasses 44 (2003) 113–116.
[12] D. Möncke, D. Ehrt, C.P.E. Varsamis, E.I. Kamitsos, A.G. Kalampounias, Glass Technol.-Part A 47 (2006) 133–137.
[13] L. Wondraczek, S. Sen, H. Behrens, R.E. Youngman, Phys. Rev. B 76 (2007) 014202 (1–9).
[14] L. Wondraczek, H. Behrens, J. Chem. Phys. 127 (2007) 154503 (1–10).
[15] L. Wondraczek, S. Krolikowski, H. Behrens, J. Non-Cryst, Solids 356 (2010) 1859–1862.
[16] B. Mantisi, S. Adichtchev, S. Sirotkin, L. Rafaelly, L. Wondraczek, H. Behrens, C. Marcenat, N.V. Surovtsev, A. Pillonnet, E. Duval, B. Champagnon, A. Mermet, J. Phys.-Condens. Mat. 22 (2010) 025402 (1–5).
[17] S. Reibstein, L. Wondraczek, D. de Ligny, S. Krolikowski, S. Sirotkin, J.P. Simon, V. Martinez, B. Champagnon, J. Chem. Phys. 134 (2011) 204502 (1–6).
[18] F. Angeli, O. Villain, S. Schuller, T. Charpentier, D. de Ligny, L. Bressel, L. Wondraczek, Phys. Rev. B 85 (2012) 054110 (1–15).
[19] A. Makishima, J.D. Mackenzie, J. Non-Cryst, Solids 12 (1973) 35–45.
[20] C.J. Phillips, Glass Technol. 5 (1964) 216–223.
[21] M.L. Williams, G.E. Scott, Glass Technol. 11 (1970) 76–79.
[22] N. Soga, J. Non-Cryst, Solids 73 (1985) 305–313.
[23] B. Bridge, N.D. Patel, D.N. Waters, Phys. Status Solidi A 77 (1983) 655–668.
[24] P.K. Gupta, J.C. Mauro, J. Chem. Phys. 130 (2009) 094503 (1–8).

[25] J.C. Phillips, M.F. Thorpe, Solid State Commun. 53 (1985) 699–702.
[26] M.M. Smedskjaer, J.C. Mauro, S. Sen, Y.Z. Yue, Chem. Mater. 22 (2010) 5358–5365.
[27] M.M. Smedskjaer, J.C. Mauro, Y.Z. Yue, Phys. Rev. Lett. 105 (2010) 115503 (1–4).
[28] M.M. Smedskjaer, J.C. Mauro, S. Sen, J. Deubener, Y.Z. Yue, J. Chem. Phys. 133 (2010) 154509 (1–6).
[29] B.P. Rodrigues, L. Wondraczek, J. Chem. Phys. 138 (2013) 244507 (1–5).
[30] T. Rouxel, C. R. Mécanique 334 (2006) 743–753.
[31] A. Arora, D.B. Marshall, B.R. Lawn, M.V. Swain, J. Non-Cryst, Solids 31 (1979) 415–428.
[32] D. Ehrt, Untersuchungen über die Verteilung von CoO und Fe₂O₃ auf die Mikrophasen des Glassystems Na₂O–B₂O₃–SiO₂, Mathematisch-Naturwissenschaftliche-Technische Fakultät, Friedrich-Schiller-Universität Jena, 1973. (Phd-thesis).
[33] A. Winterstein-Beckmann, D. Möncke, D. Palles, E.I. Kamitsos, L. Wondraczek, J. Non-Cryst, Solids 401 (2014) 110–114.
[34] A. Winterstein-Beckmann, D. Möncke, D. Palles, E.I. Kamitsos, L. Wondraczek, J. Non-Cryst, Solids 405 (2014) 196–206.
[35] R. Limbach, B.P. Rodrigues, L. Wondraczek, J. Non-Cryst, Solids 404 (2014) 124–134.
[36] Y.H. Yun, P.J. Bray, J. Non-Cryst, Solids 27 (1978) 363–380.
[37] S. Fuhrmann, Druckabhängigkeit der topologischen Heterogenität von Gläsern, Technische Fakultät Fachbereich Glas und Keramik, Friedrich-Alexander-Universität Erlangen-Nürnberg, 2013. (Phd-thesis).
[38] J.E. Shelby, Water in Glasses and Melts, The Royal Society of Chemistry, Cambridge, UK, 2005. pp. 222–236.
[39] A. Thieme, D. Möncke, R. Limbach, S. Fuhrmann, E.I. Kamitsos, L. Wondraczek, J. Non-Cryst, Solids 410 (2015) 142–150.
[40] W.C. Oliver, G.M. Pharr, J. Mater. Res. 7 (1992) 1564–1583.
[41] V. Maier, K. Durst, J. Mueller, B. Backes, H.W. Höppel, M. Göken, J. Mater. Res. 26 (2011) 1421–1430.
[42] B.N. Lucas, W.C. Oliver, Metall. Mater. Trans. A 30 (1999) 601–610.
[43] V. Maier, B. Merle, M. Göken, K. Durst, J. Mater. Res. 28 (2013) 1177–1188.
[44] L. Shen, W.C.D. Cheong, Y.L. Foo, Z. Chen, Mat. Sci. Eng. A 532 (2012) 505–510.
[45] A.F. Bower, N.A. Fleck, A. Needleman, N. Ogbonna, Proc. Roy. Soc. Lond. A 441 (1993) 97–124.
[46] R. Goodall, T.W. Clyne, Acta Mater. 54 (2006) 5489–5499.
[47] Y. Kato, H. Yamazaki, S. Yoshida, J. Matsuoka, J. Non-Cryst, Solids 356 (2010) 1768–1773.
[48] J.D. Mackenzie, J. Am. Ceram. Soc. 46 (1963) 470–476.
[49] S. Yoshida, J.C. Sangleboeuf, T. Rouxel, J. Mater. Res. 20 (2005) 3404–3412.
[50] S. Yoshida, S. Isono, J. Matsuoka, N. Soga, J. Am. Ceram. Soc. 84 (2001) 2141–2143.
[51] J.E. Neely, J.D. Mackenzie, J. Mater. Sci. 3 (1968) 603–609.
[52] K.W. Peter, J. Non-Cryst, Solids 5 (1970) 103–115.
[53] P. Sellappan, T. Rouxel, F. Celarie, E. Becker, P. Houizot, R. Conradt, Acta Mater. 61 (2013) 5949–5965.
[54] W.C. Oliver, G.M. Pharr, J. Mater. Res. 19 (2004) 3–20.
[55] M. Kodama, J. Mater. Sci. 26 (1991) 4048–4053.
[56] K. Budhwani, S. Feller, Phys. Chem. Glasses 36 (1995) 183–190.
[57] S.J. Suzuki, Y. Abe, J. Non-Cryst, Solids 43 (1981) 141–143.
[58] J.C. Mauro, P.K. Gupta, R.J. Loucks, J. Chem. Phys. 130 (2009) 234503 (1–8).
[59] A. Grandjean, M. Malki, C. Simonnet, D. Manara, B. Penelon, Phys. Rev. B 75 (2007) 054112 (1–7).
[60] M.J. Pascual, A. Duran, L. Pascual, Phys. Chem. Glasses 43 (2002) 25–31.
[61] I.G. Polyakova, E.V. Tokareva, Alkali borosilicate systems: phase diagrams and the structure of glass, in: A.C. Wright, S.A. Feller, A.C. Hannon (Eds.), Borate Glasses, Crystals and Melts, The Society of Glass Technology, Sheffield, UK, 1997, pp. 223–230.
[62] S.A. Feller, J. Kottke, J. Welter, S. Nijhawan, R. Boekenhauer, H. Zhang, D. Feil, C. Parameswar, K. Budhwani, M. Affatigato, A. Bhatnagar, G. Bhasin, S. Bhowmik, J. Mackenzie, M. Royle, M. Kambeyanda, P. Pandikuthira, M. Sharma, Physical properties of alkali borosilicate glasses, in: A.C. Wright, S.A. Feller, A.C. Hannon (Eds.), Borate Glasses, Crystals and Melts, The Society of Glass Technology, Sheffield, UK, 1997, pp. 246–253.
[63] T. Furukawa, W.B. White, J. Am. Ceram. Soc. 64 (1981) 443–447.
[64] X.W. Wu, R. Dieckmann, J. Non-Cryst, Solids 357 (2011) 2846–2856.
[65] X.W. Wu, A.K. Varshneya, R. Dieckmann, J. Non-Cryst, Solids 357 (2011) 3661–3669.
[66] X.W. Wu, R.E. Youngman, R. Dieckmann, J. Non-Cryst, Solids 378 (2013) 168–176.
[67] C.A. Maynell, G.A. Saunders, J. Non-Cryst, Solids 12 (1973) 271–294.
[68] Y. Kato, H. Yamazaki, Y. Kubo, S. Yoshida, J. Matsuoka, T. Akai, J. Ceram. Soc. Jpn. 118 (2010) 792–798.
[69] S. Yoshida, Y. Nishikubo, A. Konno, T. Sugawara, Y. Miura, J. Matsuoka, Int. J. Appl. Glass Sci. 3 (2012) 3–13.
[70] S. Yoshida, A. Hidaka, J. Matsuoka, J. Non-Cryst, Solids 344 (2004) 37–43.
[71] M. Bertoldi, V.M. Sglavo, J. Am. Ceram. Soc. 85 (2002) 2499–2506.
[72] S. Yoshida, Y. Hayashi, A. Konno, T. Sugawara, Y. Miura, J. Matsuoka, Phys. Chem. Glasses B 50 (2009) 63–70.
[73] J. Sehgal, S. Ito, J. Non-Cryst, Solids 253 (1999) 126–132.
[74] S. Sakka, J.D. Mackenzi, J. Non-Cryst, Solids 6 (1971) 145–162.
[75] R. Jabra, J. Pelous, J. Phalippou, J. Non-Cryst, Solids 37 (1980) 349–358.
[76] M. Barlet, A. Kerrache, J.M. Delaye, C.L. Rountree, J. Non-Cryst, Solids 382 (2013) 32–44.
[77] S. Inaba, S. Fujino, K. Morinaga, J. Am. Ceram. Soc. 82 (1999) 3501–3507.
[78] R.J. Eagan, J.C. Swearengen, J. Am. Ceram. Soc. 61 (1978) 27–30.
[79] C. Hermansen, J. Matsuoka, S. Yoshida, H. Yamazaki, Y. Kato, Y.Z. Yue, J. Non-Cryst, Solids 364 (2013) 40–43.
[80] A. Abd El-Moneim, Physica B 325 (2003) 319–332.

[81] S.Y. Marzouk, M.S. Gaafar, Solid State Commun. 144 (2007) 478–483.
[82] Y.B. Saddeek, L. Abd El Latif, Physica B 348 (2004) 475–484.
[83] A. Pedone, G. Malavasi, A.N. Cormack, U. Segre, M.C. Menziani, Chem. Mater. 19 (2007) 3144–3154.
[84] P. Paufler, S.K. Filatov, I.P. Shakhverdova, R.S. Bubnova, M. Reibold, B. Muller, A.A. Levin, D.C. Meyer, Glass Phys. Chem. 33 (2007) 187–198.
[85] H. Doweidar, J. Phys. Chem. Solids 53 (1992) 807–814.
[86] Q.J. Zheng, M. Potuzak, J.C. Mauro, M.M. Smedskjaer, R.E. Youngman, Y.Z. Yue, J. Non-Cryst, Solids 358 (2012) 993–1002.
[87] L.H. Kieu, J.M. Delaye, L. Cormier, C. Stolz, J. Non-Cryst, Solids 357 (2011) 3313–3321.
[88] Q. Zhao, M. Guerette, L.P. Huang, J. Non-Cryst, Solids 358 (2012) 652–657.
[89] M.S. Gaafar, S.Y. Marzouk, Physica B 388 (2007) 294–302.
[90] G.H. Frischat, W. Krause, H. Hubenthal, J. Am. Ceram. Soc. 67 (1984) C10–C12.
[91] E. Vernaz, F. Larche, J. Zarzycki, J. Non-Cryst, Solids 37 (1980) 359–365.
[92] S.M. Wiederhorn, J. Am. Ceram. Soc. 52 (1969) 99–105.
[93] E.I. Koslovskaya, Proc. Third All-Union Conference on the Glassy State 2 (1960) 299–301.
[94] N.P. Lower, R.K. Brow, C.R. Kurkjian, J. Non-Cryst, Solids 349 (2004) 168–172.
[95] T.E. Wilantewicz, J.R. Varner, J. Mater. Sci. 43 (2008) 281–298.
[96] T.E. Wilantewicz, J.R. Varner, J. Non-Cryst, Solids 354 (2008) 1553–1558.
[97] V.A. Mukhanov, O.O. Kurakevich, V.L. Solozhenko, J. Superhard, Mater. 30 (2008) 71–72.
[98] J. Ramkumar, V. Sudarsan, S. Chandramouleeswaran, V.K. Shrikhande, G.P. Kothiyal, P.V. Ravindran, S.K. Kulshreshtha, T. Mukherjee, J. Non-Cryst, Solids 354 (2008) 1591–1597.
[99] A.K. Seal, P. Chakraborti, N.R. Roy, S. Mukherjee, M.K. Mitra, G.C. Pas, B. Mater. Sci. 28 (2005) 457–460.
[100] M. Yamane, J.D. Mackenzie, J. Non-Cryst, Solids 15 (1974) 153–164.
[101] X.C. Zhang, O.L. He, C.Z. Xu, Y.H. Zheng, J Non-Cryst Solids 80 (1986) 313–318.
[102] J. de Bonfils, S. Peuget, G. Panczer, D. de Ligny, S. Henry, P.Y. Noel, A. Chenet, B. Champagnon, J. Non-Cryst, Solids 356 (2010) 388–393.
[103] L. Ainsworth, J. Soc, Glass Technol. 38 (1954) 501–535.
[104] L. Ainsworth, J. Soc, Glass Technol. 38 (1954) 536–547.
[105] Z. Burghard, A. Zimmermann, J. Rodel, F. Aldinger, B.R. Lawn, Acta Mater. 52 (2004) 293–297.
[106] H. Ishikawa, N. Shinkai, J. Am. Ceram. Soc. 65 (1982) C124–C127.
[107] R.F. Cook, G.M. Pharr, J. Am. Ceram. Soc. 73 (1990) 787–817.
[108] M. Bertoldi, V.M. Sglavo, J. Non-Cryst, Solids 344 (2004) 51–59.
[109] H. Inoue, A. Masuno, Y. Watanabe, K. Suzuki, T. Iseda, J. Am. Ceram. Soc. 95 (2012) 211–216.
[110] G.E. Jellison, L.W. Panek, P.J. Bray, G.B. Rouse, J. Chem. Phys. 66 (1977) 802–812.
[111] P.A.V. Johnson, A.C. Wright, R.N. Sinclair, J. Non-Cryst, Solids 50 (1982) 281–311.
[112] R.E. Youngman, S.T. Haubrich, J.W. Zwanziger, M.T. Janicke, B.F. Chmelka, Science 269 (1995) 1416–1420.
[113] A.C. Hannon, D.I. Grimley, R.A. Hulme, A.C. Wright, R.N. Sinclair, J. Non-Cryst, Solids 177 (1994) 299–316.
[114] J. Krogh-Moe, Phys. Chem. Glasses 6 (1965) 46–54.
[115] J. Lorösch, M. Couzi, J. Pelous, R. Vacher, A. Levasseur, J. Non-Cryst, Solids 69 (1984) 1–25.
[116] W.J. Dell, P.J. Bray, S.Z. Xiao, J. Non-Cryst, Solids 58 (1983) 1–16.
[117] M.E. Milberg, R.A. Verhelst, J.G. Okeefe, H.O. Hooper, Phys. Chem. Glasses 13 (1972) 79–84.
[118] D. Manara, A. Grandjean, D.R. Neuville, J. Non-Cryst, Solids 355 (2009) 2528–2531.
[119] A.A. Osipov, L.M. Osipova, V.E. Eremyashev, Glass Phys. Chem. 39 (2013) 105–112.
[120] M.M. Smedskjaer, J.C. Mauro, R.E. Youngman, C.L. Hogue, M. Potuzak, Y.Z. Yue, J. Phys. Chem. B 115 (2011) 12930–12946.
[121] A. Makishima, J.D. Mackenzie, J. Non-Cryst, Solids 17 (1975) 147–157.
[122] H.M. Cohen, R. Roy, Phys. Chem. Glasses 6 (1965) 149–161.
[123] J.D. Mackenzie, J. Am. Ceram. Soc. 46 (1963) 461–470.
[124] S. Susman, K.J. Volin, D.L. Price, M. Grimsditch, J.P. Rino, R.K. Kalia, P. Vashishta, G. Gwanmesia, Y. Wang, R.C. Liebermann, Phys. Rev. B 43 (1991) 1194–1197.
[125] L. Huang, J. Nicholas, J. Kieffer, J. Bass, J. Phys. Condens. Mat. 20 (2008) 075107 (1–8).
[126] A. Takada, Phys. Chem. Glasses 45 (2004) 156–159.
[127] K. Trachenko, V.V. Brazhkin, G. Ferlat, M.T. Dove, E. Artacho, Phys. Rev. B 78 (2008) 172012 (1–4).
[128] K. Hirao, Z. Zhang, H. Morita, N. Soga, J. Soc, Mater. Sci. Jpn 40 (1991) 400–404.
[129] S.K. Lee, P.J. Eng, H.K. Mao, J.F. Shu, Phys. Rev. B 78 (2008) 214203 (1–6).
[130] S. Striepe, M.M. Smedskjaer, J. Deubener, U. Bauer, H. Behrens, M. Potuzak, R.E. Youngman, J.C. Mauro, Y.Z. Yue, J. Non-Cryst, Solids 364 (2013) 44–52.
[131] R.D. Shannon, Acta Crystallogr. A 32 (1976) 751–767.
[132] T. Rouxel, H. Ji, T. Hammouda, A. Moreac, Phys. Rev. Lett. 100 (2008) 225501 (1–4).
[133] T. Rouxel, H. Ji, J.P. Guin, F. Augereau, B. Ruffle, J. Appl. Phys. 107 (2010) 094903 (1–5).
[134] E.H. Yoffe, Philos. Mag. A 46 (1982) 617–628.
[135] J. Kjeldsen, M.M. Smedskjaer, J.C. Mauro, Y.Z. Yue, Appl. Phys. Lett. 104 (2014) 051913 (1–5).
[136] J. Kjeldsen, M.M. Smedskjaer, J.C. Mauro, Y.Z. Yue, J. Non-Cryst, Solids 406 (2014) 22–26.
[137] S. Yoshida, J.C. Sangleboef, T. Rouxel, Int. J. Mater. Res. 98 (2007) 360–364.
[138] S. Yoshida, H. Sawasato, T. Sugawara, Y. Miura, J. Matsuoka, J. Mater. Res. 25 (2010) 2203–2211.
[139] T.M. Gross, J. Non-Cryst, Solids 358 (2012) 3445–3452.
[140] Z.Y. Zhang, N. Soga, K. Hirao, J. Mater. Sci. 30 (1995) 6359–6362.
[141] S. Fuhrmann, T. Deschamps, B. Champagnon, L. Wondraczek, J. Chem. Phys. 140 (2014) 054501 (1–7).

[142] D.A. Kilymis, J.M. Delaye, J. Chem. Phys. 141 (2014) 014504 (1–10).
[143] N.M. Vedishcheva, I. G. Polyakova 55 (2014) 225–336.
[144] G. Tricot, J. Trébosc, F. Pourpoint, R. Gauvin, L. Delevoye, Chapter Four — The D-HMQC MAS-NMR Technique: An Efficient Tool for the Editing of Through-space Correlation Spectra Between Quadrupolar and Spin-1/2 (^{31}P, ^{29}Si, ^{1}H, ^{13}C) Nuclei, Academic Press, 2014. 145–184.
[145] S.K. Lee, K. Mibe, Y.W. Fei, G.D. Cody, B.O. Mysen, Phys. Rev. Lett. 94 (2005) 165507 (1–4).
[146] A.C. Wright, C.E. Stone, R.N. Sinclair, N. Umesaki, N. Kitamura, K. Ura, N. Ohtori, A.C. Hannon, Phys. Chem. Glasses 41 (2000) 296–299.
[147] M. Grimsditch, A. Polian, A.C. Wright, Phys. Rev. B 54 (1996) 152–155.
[148] M.M. Smedskjaer, R.E. Youngman, S. Striepe, M. Potuzak, U. Bauer, J. Deubener, H. Behrens, J.C. Mauro, Y.Z. Yue, Sci. Rep. UK 4 (2014) 3770 (1–6).
[149] S.K. Lee, P.J. Eng, H.K. Mao, Y. Meng, M. Newville, M.Y. Hu, J.F. Shu, Nat. Mater. 4 (2005) 851–854.
[150] K. Hirao, J. Matsuoka, N. Soga, J. Non-Cryst, Solids 112 (1989) 336–340.
[151] D. Tabor, Rev. Phys. Tech. 1 (1970) 145–179.
[152] W.P. Yu, J.P. Blanchard, J. Mater. Res. 11 (1996) 2358–2367.
[153] N.A. Sakharova, J. Fernandes, J.M. Antunes, M.C. Oliveira, Int. J. Solids Struct. 46 (2009) 1095–1104.
[154] B.R. Lawn, M.V. Swain, J. Mater. Sci. 10 (1975) 113–122.
[155] D.B. Marshall, B.R. Lawn, A.G. Evans, J Am Ceram Soc 65 (1982) 561–566.
[156] W.D. Nix, H.J. Gao, J. Mech, Phys. Solids 46 (1998) 411–425.
[157] T.M. Gross, M. Tomozawa, J. Non-Cryst, Solids 354 (2008) 5567–5569.
[158] L. Shartsis, W. Capps, S. Spinner, J. Am. Ceram. Soc. 36 (1953) 35–43.
[159] J.T. Hagan, J. Mater. Sci. 14 (1979) 462–466.
[160] J.T. Hagan, M.V. Swain, J. Phys. D 11 (1978) 2091–2102.
[161] B.R. Lawn, D.B. Marshall, J. Am. Ceram. Soc. 62 (1979) 347–350.
[162] J.J. Lewandowski, W.H. Wang, A.L. Greer, Phil. Mag. Lett. 85 (2005) 77–87.
[163] W. Haller, D.H. Blackburn, F.E. Wagstaff, R.J. Charles, J. Am. Ceram. Soc. 53 (1970) 34–39.